Journal of Materials Chemistry C

Accepted Manuscript

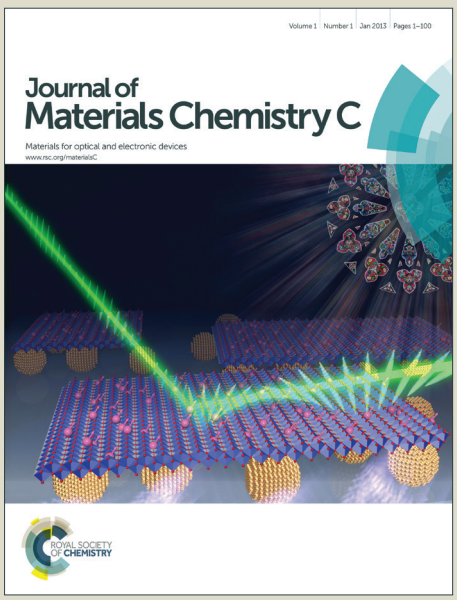

ROYAL SOCIETY OF CHEMISTRY

www.rsc.org/materialsC

Journal Name

RSCPublishing

ARTICLE

Nd_2O_3/Au nanocomposites: Upconversion Broadband Emission and Enhancement under Near-infrared Light Excitation

Cite this: DOI: 10.1039/x0xx00000x

Received 00th January 2012,
Accepted 00th January 2012

DOI: 10.1039/x0xx00000x

www.rsc.org/

Xu Chen[a], Wen Xu*[a], Yongsheng Zhu[a,b], Pingwei Zhou[a], Shaobo Cui[a,b], Li Tao[a], Lin Xu[a], Hongwei Song*[a]

Abstract

In the present work, a novel strategy of Nd_2O_3/Au nanocomposites has been successfully synthesized by a co-precipitation process, in which the upconversion luminescence (UCL) of Nd_2O_3 was a white broadband emission under 780-980 nm excitation. The UCL enhancement in Nd_2O_3/Au nanocomposites with different doped concentration of Au nanorods (NRs), under 980 nm and 808 nm excitation was systemically studied. It's observed that through the interaction of Nd_2O_3 with surface plasmon (SP) of Au NRs, the threshold power for generating broadbands was suppressed largely in contrast to the Nd_2O_3 nanoparticles (NPs). Further, it is interesting to observe that the enhancement is strongly dependent on the doped concentration of Au NRs and the excitation power of 980 nm and 808 nm laser diodes. The optimum UCL enhancement is 11-fold and 9-fold under 980 nm and 808 nm excitation, respectively. In addition, the upconversion (UC) broad band emission and UCL enhancement mechanism of Nd_2O_3/Au nanocomposites were proposed.

1. Introduction

In recent years, infrared-to-visible frequency upconversion emission in rare earth (RE)-doped nanocrystals has become a major scientific interest, owing to its potential applications in bio-label, lasers, solar cell, three-dimensional solid-state multi-color display, and so on.[1-6] At present, one of the most efficient UCL materials, based on 4f-4f sharp line transitions of trivalent lanthanide ions, is rare earth ions co-doped fluoride phosphors (such as $NaYF_4:Yb^{3+}$: Er^{3+} or Yb^{3+}: Tm^{3+}) under 980 nm excitation, because these fluoride phosphors have lower phonon threshold and their energy levels matched to the excitation light effectively.[7,8] However, their upconversion efficiency is still low, which can not satisfy the requirement of various practical applications. For instance, bulk $NaYF_4$:Yb^{3+}, Er^{3+} in hexagonal phase, is commonly considered as the most efficient upconversion phosphor, whose efficiency is only 3%. And the strength of corresponding nanosized phosphor (<20 nm) is only one of tenth of the bulk.[9,10] Until now, it is still a challenge to obtain highly efficient upconversion phosphors.

Up to now, there are a few reports about the efficient UC broad emission, especially in the rare earth oxides. These excellent rare earth oxides are chemically, photothermally, and photochemically stable, and have stronger upconvertion luminescence. For example, Wang et al. observed efficient UC broadband emission in Yb_2O_3, Sm_2O_3, and the upconversion efficiency was estimated to be as high as 10 %, and they attributed the broad band emissions to thermal avalanche.[11] Further works were performed to indentify the origin of the broad band emissions by Strek et al. and Wang et al.[12,13] Strek attributed the broad band emissions to the charge transfer transition of Yb^{3+}. Recently, our group observed that some lanthanide oxides, such as Er_2O_3, Sm_2O_3, Nd_2O_3 and Pr_2O_3 demonstrated not only sufficient upconversion broad bands, but also sufficient infrared broad bands, ranging of 1000-1700 nm under 980 nm excitation.[14]

How to improve the efficiency of UCL is still one of the most important efforts that should be made. Many methods have been

explored.[15-19] One of the most efficient methods is the coupling of the emitters to the noble metal nanostructures, which generated strong surface plasmon absorption (SPA). To date, a lot of works mainly focused on improving the UCL efficiency of rare earth ions co-doped fluoride phosphors (such as $NaYF_4$:Yb^{3+} : Er^{3+} or $NaYF_4$:Yb^{3+}: Tm^{3+}) through the coupling of nanophosphors to the SPA of noble metal nanostructures (silver and gold).[20-24]

However, there are few reports about the modulation on the UC broadband emission of rare earth with the noble metal. In the present work, we reported the synthesis of novel Nd_2O_3/Au nanocomposites, and systemically studied the UCL enhancement with different doped concentration of Au NRs, under 980 nm and 808 nm excitation. It is interesting to observe that in the composites, the optimum UCL enhancement is 11-fold and 9-fold under 980 nm and 808 nm excitation, respectively, depending on the doped Au NRs concentration and the excitation power density. Furthermore, the UC broadband emission and UCL enhancement mechanism of Nd_2O_3/Au nanocomposites were proposed.

2. Experimental

2.1 Synthesis of Au NRs.

The Au NRs were prepared according to the seed-mediated growth method, reported by EI-Sayed and co-workers.[25] Firstly, the seed solution was prepared by mixing 7.5 mL of CTAB (0.1 M) and 2.5 mL of $HAuCl_4$ (1 mM) with 0.6 mL of prepared 10 mM $NaBH_4$ solution under vigorously stirring at 27 °C. After 2 hours, the seed solution was used for the synthesis of the Au NRs. Secondly, 66 mL of 0.1 M CTAB was mixed with 60 mL of 1 mM $HAuCl_4$, then 1.2 mL of 0.01 mM silver nitrate aqueous solution and 1.1 mL of 2 M hydrochloric acid were added to a 250 mL flask. After gently mixing the solution to 2 hours, 0.96 mL of 0.1 M Ascorbic Acid and 1 mL of the as-synthesized seed solution were simultaneously added to initiate the growth of the Au NRs. These NRs were aged 5 hours to ensure full growth at 27 °C. Finally, after preparation, excess CTAB was removed by centrifuging at 12 000 rpm for 15 min, and then re-dispersed in 10 mL deionized water.

2.2 Synthesis of Nd_2O_3/Au nanocomposites.

0.504 g of $Nd(NO_3)_3 \cdot 6H_2O$ and 2.4 g urea were dissolved in 40 mL of deionized water in a flask with stirring until the solution became homogenous. Then, different volume of the pre-synthesized Au NRs aqueous solution was added into the above $Nd(NO_3)_3$ and urea solution. After that, the obtained solution was heated to 90 °C and kept for one hour in the water bath with refluxing.[26] The resulting suspension was separated by centrifugation (8000 rpm,12 min) and collected after washing with alcohol for three times. Then the as-synthesized products （$Nd(OH)CO_3$/Au） were dried at 80 °C for 3 hours, and sintered in air at 900 °C for 3 hours to obtain the Nd_2O_3/Au nanocomposites. For further comparison, the Nd_2O_3 NPs were also synthesized

2.3 Characterization

The morphology of the products was recorded on a Hitachi H-8100IV transmission electron microscope (TEM) under an acceleration voltage of 200 kV and scanning electron microscope (SEM). The energy-dispersive X-ray (EDX) elemental mapping images were recorded on a FEI Tecnai G2 S-Twin microscope under a working voltage of 200 kV equipped with EDX spectrometer. The phase structure and purity of the as-prepared samples were characterized by X-ray power diffraction (XRD) with a Rigaku D/max 2550 X-ray diffractometer, using a monochromatized Cu target radiation resource (λ=1.54 Å). UV/Vis–NIR absorption spectra were measured with a Shimadzu UV-1800PC UV/Vis–NIR scanning spectrophotometer in the range from 300 to 1100 nm. In the measurements of power-dependent UCL spectra, a continuous 980 nm or a 808 nm light diode was used to pump the samples. A visible photomultiplier (350–850 nm) combined with a double-grating monochromator was used for spectral collection. In order to obtain the excitation spectra of UCL, the integrated intensity over the 350-720 nm range of the emission was plotted versus excitation wavelength, and that process was fulfilled by using a Titanium: Sapphire oscillator (Mira-HP; Coherent, Santa Clara, CA) which worked in the CW mode which was pumped by a continuous wave laser (Verdi-V18; Coherent). The photo current-voltage (I-V) curves were acquired by a source-measurement unit under the illumination of continuous 980 nm diode laser or Titanium: Sapphire oscillator which worked in the CW mode (790 ~ 830 nm).

3. Results and discussion

3.1 Morphology and structure

Firstly, Fig. 1 (a-d) show the SEM image of the oxide precursors and the calcined Nd_2O_3/Au nanocomposites. The oxide precursors of basic carbonate composites were synthesized by co-precipitation method.[26] Then the oxide precursors were converted to the oxides during the subsequent calcination process as gradual elimination of H_2O and CO_2 by thermal decomposition at 900 °C. Fig. 1(a-d) represent the SEM images of $Nd(OH)CO_3$, Nd_2O_3, $Nd(OH)CO_3$/Au composites and Nd_2O_3/Au composites, respectively. It can be seen that, the morphology of as-prepared $Nd(OH)CO_3$ and $Nd(OH)CO_3$/Au composites are both rod-like and monodisperse, the length of Nd_2O_3 NPs is about 0.8-1.0 μm, while it's diameter is 0.2-0.3 μm. After the calcination process, the samples have a degree of agglomeration. Because of the large size and large contrast of Nd_2O_3, we can not observe the internal structure of Nd_2O_3/Au. Fig. 1(e) displays XRD patterns of the Nd_2O_3/Au composites of different doped concentration of Au NRs. It can be seen that most of the diffraction peaks agreed with the standard card JCPDS 41-1089 of cubic phase Nd_2O_3. Because the amount of Au is relatively low compared to the Nd element, only as the doped concentration of Au NRs was larger than 7.5 μmol, a new XRD peak located at 2θ = 38.2° was observed, which was assigned to the characteristic diffraction peak (111) of cubic gold (JCPDS No. 04-0784), as shown in Fig.1 (f). It implied the formation of Nd_2O_3/Au composites. Furthermore, the morphology of Au NRs was also examined by TEM in Fig.1 (g), which indicated that the Au NRs were uniform and

monodisperse, with an average diameter of ~20 nm and length of ~50 nm.

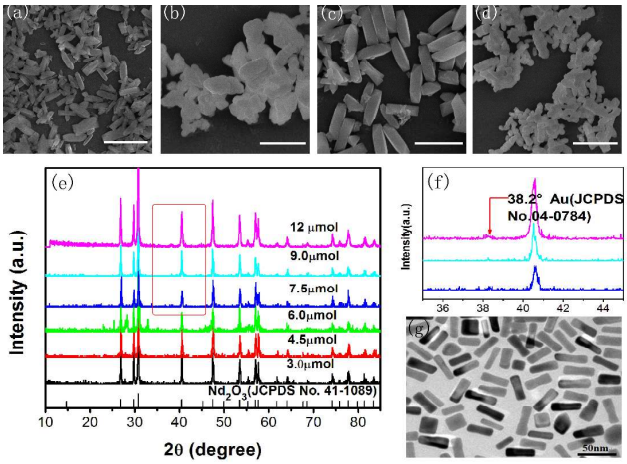

Fig.1 (a-d) SEM images of the precursor (Nd_2O_3), the calcined Nd_2O_3, Nd_2O_3/Au composites and the calcined Nd_2O_3/Au composites (1μm); (e) the XRD patterns of the calcined Nd_2O_3, and the calcined Nd_2O_3/Au composites with different doped concentration of Au nanorods(3.0 μmol-12 μmol); (f) the XRD patterns of the calcined Nd_2O_3/Au composites (7.5 μmol-12 μmol); (g) TEM image of the prepared gold nanorods.

In order to further identify the internal structure of the Nd_2O_3/Au composites, HR-TEM image and the corresponding EDX mapping of Nd_2O_3/Au sample (the concentration of Au NRs is 6 μmol) were detected to analysis the elements, as shown in Fig.2 (a-d). Fig.2 (b-d) represent the mappings of neodymium, oxygen, and gold elements, respectively. It can be seen that all of the elements distribute homogeneously in the sample. This indicates that the Au NRs have been diffused after being annealed at 900 ^{o}C. In Fig.2(e), two different fringe spacings were determined to be ~0.33 nm and ~0.235 nm, which corresponded closely to the spacings of the (100) plane of cubic Nd_2O_3 (0.33 nm) (JCPDS No.41-1089) and the (111) plane of fcc gold (0.235 nm) (JCPDS No.04-0784), respectively. From the EDX mapping and the TEM, we can further confirm the formation of Nd_2O_3/Au nanocomposites.

Fig.3 shows the absorption spectra of Au NRs, and Nd_2O_3/Au composites under different doped concentrations of Au NRs, respectively. It can be seen that there are two absorption peaks in Au NRs, and the central locations are at 525 nm and 810 nm, corresponding to the transverse and longitudinal modes of localized SPA of Au NRs, respectively.[27] In the Nd_2O_3/Au samples, the broad bands of absorption were identified, extending of 350-1100 nm. It is interesting to observe that the absorption location gradually shifted to long wavelength side (shifted from 580 to 750 nm) as the doped concentration of Au NRs increased from 0 to 6 μmol, as the doped concentration of Au NRs further increased, the absorption peak gradually shifted to short wavelength side (shifted from 750 to 500 nm). Because the longitude SPA of Au was observed, it suggests that, in Nd_2O_3/Au composites, the Au NRs might be changed into the small NPs, which demonstrate anisotropic. It is suggested that as the dopedconcentration of Au NRs is relatively low, ranging of 0-6 μmol, due to the amount of Au NPs increases, the absorption

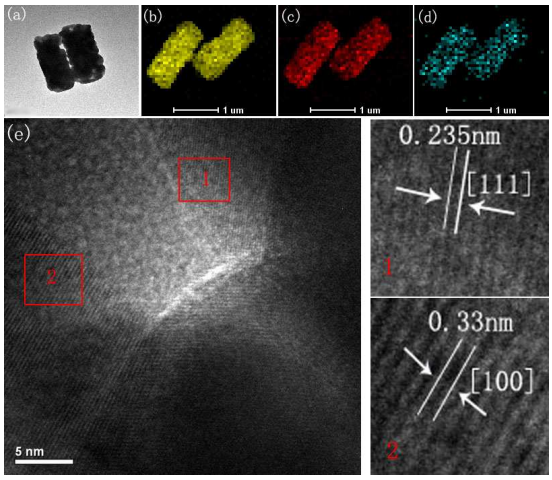

Fig.2 (a) TEM images of Nd_2O_3/Au nanocomposites; (b-d) the energy-dispersive X-ray (EDX) mapping of Nd_2O_3/Au sample at the top of the figure; (e) the HR-TEM images of Nd_2O_3/Au nanocomposites.

location of Nd_2O_3/Au composites shifts to the long wavelength due to the improved interaction of Au NPs.[28] And further increase the doped concentration of Au NRs, the Au maybe aggregate together, and the interaction distance between Au NPs is too close, leading to the absorption peak shift toward the short wavelength. This suggests that the doped concentration of Au NRs has a very important effect on the absorption of Nd_2O_3/Au.

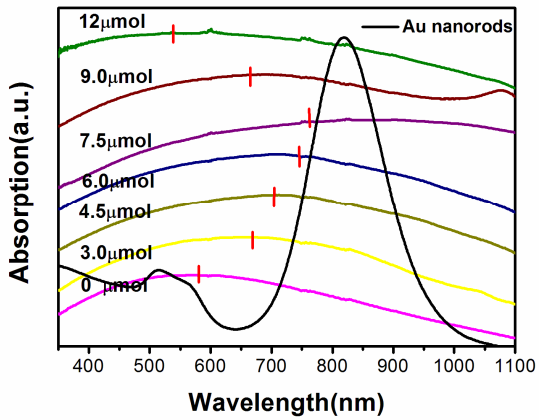

Fig.3 The absorption spectra of Au NRs and Nd_2O_3/Au nanocomposites doped 0-12 μmol Au NRs.

3.2 UCL enhancement of Nd_2O_3/Au nanocomposites

Fig.4 (a-d) show the UCL spectra of Nd_2O_3 NPs and Nd_2O_3/Au nanocomposites under the excitation of 0.42-1.18 W/mm^2 980 nm light, with the doped Au NRs concentration of 0, 3, 6 and 12 μmol, respectively. From Fig.4 (a), it can be seen that, it displays four significant groups of intrinsic emission lines of Nd^{3+}. The line in the

green range corresponds to the $^4G_{9/2}$-$^4I_{11/2}$ transition, while those in the red range to the $^4G_{11/2}$-$^4I_{13/2}$, $^4G_{9/2}$-$^4I_{15/2}$, $^4G_{5/2}$-$^4I_{13/2}$ transitions, respectively.[14] In Fig.4 (b-d), the intrinsic emissions of Nd^{3+} significantly reduce in Nd_2O_3/Au composites, with the doped concentration approaches to 6 μmol, the emission lines almost disappear. Further, it's interesting to observe that a broad band emission ranging of 400-800 nm appears for both Nd_2O_3 and Nd_2O_3/Au composites, their central position locates at about 600 nm (2.0 eV), independent of the excitation power and the Au NRs concentration. It should be highlighted that in contrast to Nd_2O_3 NPs, the threshold power of generating white broad bands in the Nd_2O_3/Au nanocomposites degraded from 0.65 W/mm^2 to 0.42 W/mm^2. In our previous work,[14] in bulk Nd_2O_3, the generation of broad bands originates from the contribution of different transitions of Nd^{3+} ions, $^4G_{9/2}$-$^4I_{11/2}$, $^4G_{11/2}$-$^4I_{13/2}$, $^4G_{9/2}$-$^4I_{15/2}$ and $^4G_{5/2}$-$^4I_{13/2}$ and their spectra broadening, which is completely different from the broad band emissions demonstrated in this work. The broad band emissions of Nd_2O_3 and Nd_2O_3/Au composites located at 600 nm (2.0 eV), are independent on excitation power and Au NRs concentration, which is very similar to our previous result observed in YVO_4: Yb^{3+}, Er^{3+} NPs.[29] It could be attributed to the UCL of oxygen defects. In fact, the broad band UC emissions in lanthanide oxides are still quite complex and their generation mechanism has not been clarified. Generally, they may be attributed to charge transfer transitions of rare earths, oxygen defect transitions, or electron-hole pairs.[12,30,31] The mechanism will be discussed later in details.

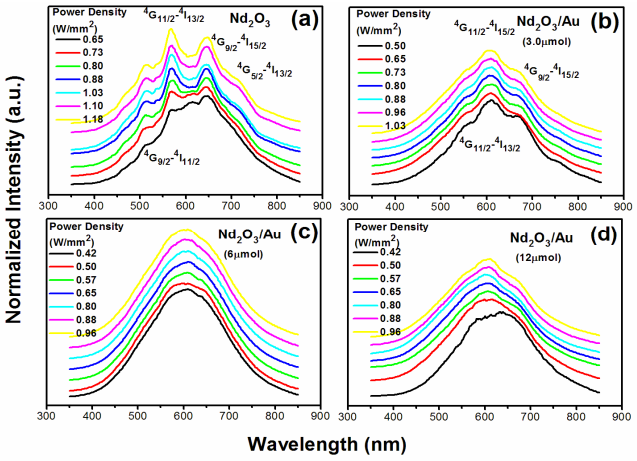

Fig.4 (a-d) The UCL spectra of Nd_2O_3, and Nd_2O_3/Au nanocomposites doped 3, 6, and 12 μmol Au NRs as a function of 980 nm excitation power, respectively.

In addition, the UCL spectra of Nd_2O_3 NPs and Nd_2O_3/Au composites were investigated under the 808 nm excitation, with changing the excitation power and the Au NRs concentration, shown in Fig.5 (a-d). It can be seen that the intrinsic spectra of Nd^{3+} ions have been identified corresponding to the $^4G_{9/2}$-$^4I_{11/2}$, $^4G_{11/2}$-$^4I_{15/2}$, and $^4G_{9/2}$-$^4I_{15/2}$ transitions, respectively. The intrinsic emissions of Nd^{3+} almost disappear in Nd_2O_3/Au composites, with the doped concentration approaches to 6 μmol, which is similar to the phenomenon observed under 980 nm excitation. They also demonstrate broad band emission ranging of 400-750 nm, and the central emissions locate at around 650 nm. It's worth noting that the central position of broad band emission of Nd_2O_3/Au composites under 808 nm excitation locates at 600 nm as the excitation power is high enough, which is similar to be observed under 980nm excitation. In contrast to Nd_2O_3 NPs, the threshold power of generating white broad bands in the Nd_2O_3/Au nanocomposites also degraded from 0.28 W/mm^2 to 0.19 W/mm^2 under 808 nm excitation.

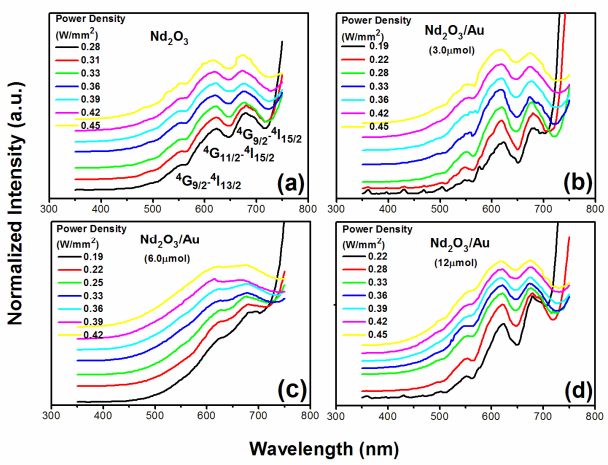

Fig.5 (a-d) The UCL spectra of Nd_2O_3 and Nd_2O_3/Au nanocomposites doped 3, 6, and 12 μmol Au nanorods as a function of 808 nm excitation power, respectively.

The power-dependent UCL properties of Nd_2O_3 NPs and Nd_2O_3/Au nanocomposites were also studied and compared under 980 nm and 808 nm excitation, as shown in Fig.6. The UCL intensity (I_{UC}) increases with the increasing excitation power (P), with a power law of $I \sim P^n$, where n represents the number of pumping photons required to excite rare earth ions from the ground state.[32] From Fig.6 (a), it can be seen that, under 980 nm excitation, the slope n was deduced that n=5.25 for Nd_2O_3 NPs, with the increasing of the doped concentration of the Au NRs, ranging of 3-12 μmol, the slope n *of* Nd_2O_3/Au nanocomposites are 1.99, 1.26, and 2.91, respectively. The slope of Nd_2O_3/Au nanocomposites is lower than that of Nd_2O_3, which would be attributed to the saturation effect and photo-induced thermal effect.[33,34] In addition, the power-dependent UCL behavior of Nd_2O_3 NPs and Nd_2O_3/Au nanocomposites under the excitation of 808 nm is shown in Fig.6 (c). For Nd_2O_3, the slope is assigned to 6.53, and in the Nd_2O_3/Au composites, as the Au NRs concentration changes from 3 μmol to 12 μmol, the slopes are 6.97, 5.51, 7.2, respectively. In most of cases, the slope n represents the photon number of a two-photon or multi-photon process. However, it is not an absolute rule, for instance, when photon avalanche or pumping saturation effect happens, the value of n may be also much larger than the photon number, or much smaller than the photon number.[33,34] Presently,

the super-strong and complex power dependence on the UCL intensity has not been completely understood. It is suggested that during the UC process, photon avalanche or thermal avalanche probably happens.[11] Fig.6 (b) and Fig.6 (d) show the UCL enhancement factor (EF, which is defined as the ratio of UCL intensity of the Nd_2O_3/Au nanocomposites to that of Nd_2O_3 NPs) as a function of excitation power under 980 nm and 808 nm excitation, respectively. It is interesting to observe that the EF varies significantly with the Au NRs concentration and excitation power.

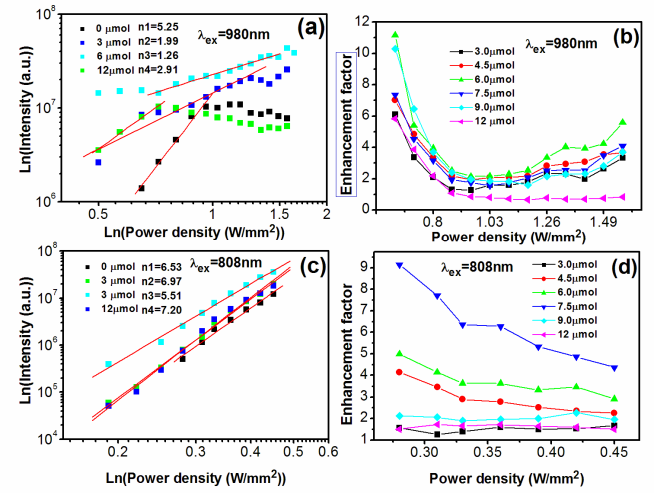

Fig.6 (a) The power dependence of integral UCL intensity of Nd_2O_3 NPs, Nd_2O_3/Au doped 3, 6, and 12 μmol Au NRs on excitation power of 980 nm light; (b) the UCL EF as a function of excitation power under 980 nm excitation; (c) the power dependence of integral UCL intensity of Nd_2O_3, and Nd_2O_3/Au nanocomposites doped 3, 6, and 12 μmol Au nanorods on excitation power of 808 nm light; (d) the UCL EF as a function of excitation power under 808 nm excitation.

In Fig.6 (b), at relatively low excitation power (980 nm, ~0.65 W/mm^2), the UCL of Nd_2O_3/Au nanocomposites was stronger than that of Nd_2O_3 NPs. The EF is about 5-11 fold with the Au NRs concentration ranging of 3-12 μmol. In detail, the EF first increases, as the Au NRs concentration approaches to 6-8 μmol, the EF approaches to the maximum, then decreases. As the excitation power increases, EF gradually decreases. From Fig.6 (d), it can be seen that, under 808 nm excitation, the EF is also strongly dependent on the Au NRs concentration and excitation power. The optimal EF is 9-fold, as the Au NRs concentration is 7.5 μmol. And with increasing the excitation power, the EF gradually decreases. From the results, we can know that the EF has an optimum, when the Au NRs concentration is about 6-8 μmol and the excitation power is low. As shown in Fig.3, the absorption peak first red-shifts as the Au NRs concentration is 3-6 μmol, then with the concentration exceeds the 7.5 μmol, the absorption peak bule-shifts. These phenomena match with UCL enhancement in Nd_2O_3/Au nanocomposites. That is to say, as the Au NRs concentration is 6-8 μmol, the excitation wavelength is closer to the absorption peak, leading to the higher EF. In general, the UCL enhancement of Nd_2O_3/Au composites could be possibly due to three reasons: first, under 980 nm or 808 nm excitation, corresponding to the longitude SPA of Au NPs, ET from Ag NPs to Nd_2O_3 may happen; second, the excitation and emission strength increase due to the field enhancement effect; third, the thermal effect happened with the surface plasmon excitation of Au NPs, leading to the thermal avalanche happening easily, and to the decrease of excitation threshold of the broadband emission.

In order to clarify the origin of the UCL enhancement, the excitation spectra in a range of 780-860 nm in Nd_2O_3 powders and Nd_2O_3/Au nanocomposites (6 μmol) were measured and compared, as shown in Fig.7. It is interesting to observe that, in both Nd_2O_3 powders and Nd_2O_3/Au nanocomposites, the UCL of the broadband was obtained not only under the excitation of 980 nm, corresponding to the excitation of $^4I_{9/2}$-$^4F_{3/2}$ transition of Nd^{3+} ions, but also under the excitation of 780-860 nm laser light, corresponding to the excitation of $^4I_{9/2}$-$^4F_{5/2}$ transition of Nd^{3+} ions. It should be noted that the broad band UC emissions are all the same and exactly in accordance with that under 980 nm excitation at the high excitation power. In Nd_2O_3 powders, the excitation bands were identified, centering around 810 nm, and for Nd_2O_3/Au nanocomposites, the excitation bands blue-shifted to 790 nm. And the absorption location of the Nd_2O_3/Au nanocomposites is about 750 nm. This implies that because of the longitude SPA of Au NPs, there may be ET from Au NPs to Nd_2O_3 to a certain extent, leading to the excitation band blue-shift of Nd_2O_3/Au composites. In addition, in Nd_2O_3/Au composites, the UC enhancement of the intrinsic transitions of Nd^{3+} was not detected instead of quenching. Because both the ET from Au NPs to Nd_2O_3 and the field enhancement effect would lead to increase of the intrinsic transitions of Nd^{3+}, so it can be deduced that the main UCL enhancement mechanism would be due to the thermal effect with the surface plasmon excitation of Au NPs, which lead to the thermal avalanche happen easily, and decrease the excitation threshold of broad emission. Furthermore, the ET may exist, but it is not a main reason.

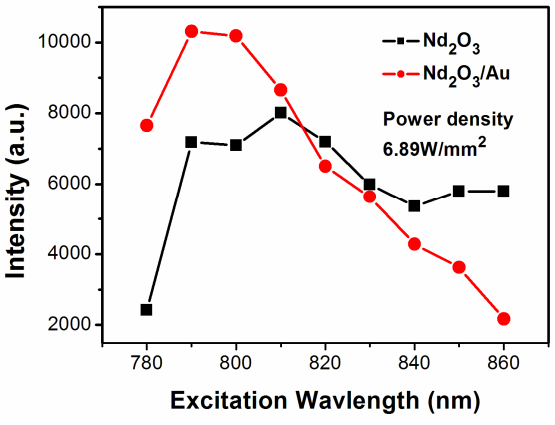

Fig.7 The UC excitation spectra in a range of 780-860 nm in Nd_2O_3 NPs and Nd_2O_3/Au nanocomposites.

4. The origin of UC broadband emission

In order to better understand the formation mechanism of the UC broad band process, the temperature as a function of excitation power was achieved by burying a thermocouple thermometer into the powder plate samples in the Nd_2O_3 NPs and Nd_2O_3/Au composites (doped with 3 μmol, 6 μmol, and 12 μmol Au NRs) under 980 nm and 808 nm excitation, respectively. The results were shown in Fig.8. It can be seen that in all the samples, the temperature increases with the increasing of the excitation power in the range of 380-700 K. In Fig.8 (a), under 980 nm excitation in Nd_2O_3 NPs, the temperature increases from 399 K to 614 K under the excitation power ranging from 0.65 W/mm^2 to 1.87 W/mm^2, and in the Nd_2O_3/Au nanocomposites, the temperature varies from 380 K to 673 K under the excitation power ranging from 0.42 W/mm^2 to 1.87 W/mm^2. It is suggested that, Nd_2O_3/Au

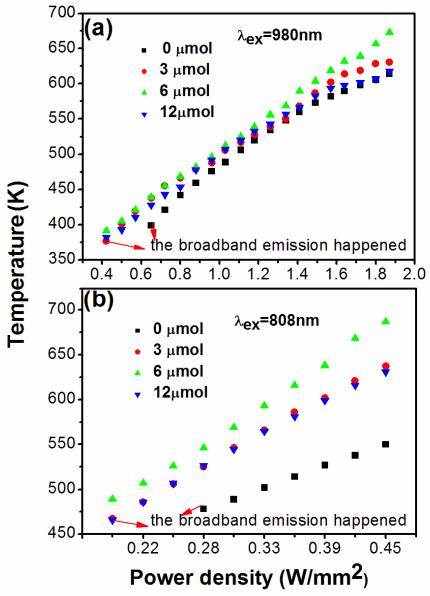

Fig.8 The temperature as a function of excitation power in the Nd_2O_3 NPs and Nd_2O_3/Au nanocomposites samples doped 3, 6, and 12 μmol Au nanorods under 980 nm(a) and 808 nm(b) excitation

nanocomposites have higher temperature than that of Nd_2O_3 NPs and the threshold power of generating white broad bands in the Nd_2O_3/Au nanocomposites (0.42 W/mm^2) is lower than that for the Nd_2O_3 sample (0.65 W/mm^2). And the temperature of the sample doped 6 μmol Au NRs is the highest, which is consistent with the UC broad band enhancement. And it further confirmed that the UCL enhancement would come from the thermal effect. In addition, the temperature of broad band emission happening is about 390 K for all the samples (the necessary temperature for generating holes in the valence band). Fig.8 (b) records the temperature under 808 nm excitation in Nd_2O_3 NPs and Nd_2O_3/Au composites. The behavior is similar to that of under 980 nm excitation. In Nd_2O_3, the temperature increases from 478 K to 550 K under the excitation power ranging from 0.28 W/mm^2 to 0.45 W/mm^2, and in Nd_2O_3/Au nanocomposites, the temperature varies from 470 K to 687 K under the excitation power ranging from 0.19 W/mm^2 to 0.45 W/mm^2. The Nd_2O_3/Au nanocomposites have higher temperature than that of Nd_2O_3 NPs and the threshold power of generating white broad bands in the Nd_2O_3/Au nanocomposites (0.19 W/mm^2) is lower than that for the Nd_2O_3 sample (0.28 W/mm^2). In addition, the temperature of broad band emission happening is about 480 K for the samples. And the temperature of the sample doped 6 μmol Au NRs is the highest. Above all, they indicated that the occurrence of the broad band UCL is related to the thermal effect of the Au NPs and generate the thermal holes in valence band. It should be noted that the temperature is much lower than the temperature necessary for generating sufficient blackbody radiation (~2500 K).[29] Further, the photocurrent as a function of excitation power in Nd_2O_3 NPs and Nd_2O_3/Au nanocomposites samples under 980 nm excitation were also studied. The photocurrent increases with the increasing of the excitation power, which is along with generating the UC broad band. In Nd_2O_3 NPs, the photocurrent increases from 0 nA to 150 nA, and in Nd_2O_3/Au nanocomposites, the photocurrent increases from 0 nA to 300 nA, which is higher than that of Nd_2O_3 NPs.

Fig.9 shows the schematic of the possible mechanism of UC broadband emission in Nd_2O_3 NPs and UCL enhancement in Nd_2O_3/Au nanocomposites. In the Nd_2O_3 NPs, Nd^{3+} ions on ground states $^4I_{9/2}$ are easily excited to $^4F_{3/2}$ and $^4F_{5/2}$ by the first-step ET from excited Nd^{3+} under 980 nm or 780-860 nm excitation. And then are excited to $^4G_{11/2}$, $^2D_{5/2}$ by the second-step ET or excited-state absorption, respectively, subsequent nonradiative relaxation of $^4G_{11/2}$, $^2D_{5/2}$ populate to the $^4G_{5/2}$, $^4G_{7/2}$, $^4G_{9/2}$ and $^4G_{11/2}$ levels. At the low power excitation, the electrons stepwise populate to the $^4I_{11/2}$, $^4I_{15/2}$, and $^4I_{13/2}$ subsequently generating the blue, green and red emissions. And the exposure with high power induces the temperature of Nd_2O_3 NPs or Nd_2O_3/Au nanocomposites samples increasing considerably, leading to the cross relaxation ($^4F_{7/2}$+$^4G_{11/2}$→ $^4G_{5/2}$+$^4G_{5/2}$) exacerbate. Because the multi-photon (n>3) UCL was not observed in Nd_2O_3 NPs or Nd_2O_3/Au nanocomposites, we can confirm that most of the electrons on $^4G_{5/2}$ are captured by the oxygen vacancy states through the tunneling effect. Meantime, in the valence band of Nd_2O_3 NPs or Nd_2O_3/Au nanocomposites, a large number of holes were generated, which could be confirmed by the occurrence of photocurrent and the fact that most of other RE_2O_3 compounds were p-type semiconductors.[35] The electrons on oxygen vacancy states recombined with holes in the valence band of Nd_2O_3, generating the broad band UCL. It should be pointed out that the radiative transition rate of electron-hole recombination of semiconductor was at least several orders larger than the 4*f*-4*f* transitions of Nd^{3+} ions,[36,37] and thus could exceed the nonradiative relaxation rate of Nd^{3+} ions, preventing the thermal quenching of UCL. On the contrary, due to the direct 4*f*-4*f* radiative transition rate of excited Nd^{3+} ions was much smaller than the nonradiative relaxation rate at elevated temperature, this kind of UCL was unavoidably quenched.

And in Nd_2O_3/Au nanocomposites, the improvement of UCL are mainly attributed to the thermal effect with the surface plasmon excitation of Au NPs which is beneficial to generating thermal holes in the valence band, resulting in the decrease of threshold power for generating white light.

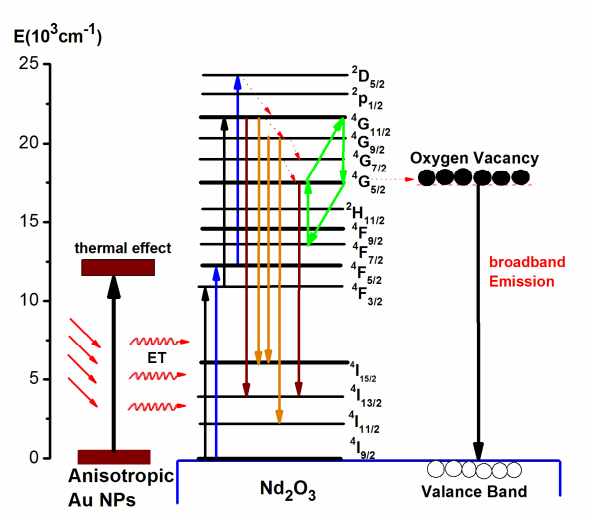

Fig.9 The schematic of the possible mechanism of the broad band UC emission in Nd_2O_3 NPs and UCL enhancement in Nd_2O_3/Au nanocomposites

Conclusions

In summary, we designed and obtained a novel type of UC nanocomposites, Nd_2O_3/Au, with broad visible emissions (400-800 nm) under 780-980 nm excitation, which differs from the previous lanthanide compound UCPs. The results show that in the composites anisotropic Au NPs distribute randomly in the composites and have strong SPA in the range of 400-1000 nm. And UCL intensity of Nd_2O_3/Au composites was improved more greatly than that of Nd_2O_3 NPs, depending strongly on the doped concentration of Au NRs and the excitation power of 980 nm and 808 nm laser diodes. The optimum enhancement of Nd_2O_3/Au composites under 980 nm and 808 nm is 11-fold and 9-fold, respectively. The mechanism of the UC broad band emission in Nd_2O_3 and Nd_2O_3/Au composites was attributed to the electron-hole combination and the UCL enhancement in Nd_2O_3/Au composites was mainly attributed to thermal effect, which dramatically increased the density of holes on the valence band.

Acknowledgements

This work was supported by the Major State Basic Research Development Program of China (973 Program) (No. 2014CB643506), the National Natural Science Foundation of China (Grant No. 11374127, 11304118, 61204015, 81201738, 61177042, and 11174111), Program for Chang Jiang Scholars and Innovative Research Team in University (No. IRT13018).

Notes and references

[a]*State Key Laboratory on Integrated Optoelectronics, College of Electronic Science and Engineering, Jilin University, 2699 Qianjin Street, Changchun 130012, China.*
[b]*College of Physics, Jilin University, 2699 Qianjin Street, Changchun 130012, China.*
Email: wen_xu09@163.com, songhw@jlu.edu.cn.

1. F. Wang, D. Banerjee, Y. S. Liu, X. Y. Chen, X. G. Liu, *Analyst*, 2010, **135**, 1839–1854.
2. R. Yan; Y. Li, Adv. *Funct. Mater.*, 2005, **15**, 763.
3. F. Auzel, *Chem. Rev.* 2004, **104** , 139.
4. A. Shalav, B. S. Richards, T. Trupke, K. W. Kramer, H. U. Gudel, *Appl.Phys. Lett.,* 2005, **86**, 01350.
5. D.Q. Chen, Y.S. Wang, K.L. Zheng, T.L. Guo, Y.L. Yu, P. Huang, *Appl. Phys. Lett.,* 2007, **91**, 251903.
6. E. Downing, L. Hesselink, J. Ralston, and R. MacFarlane, *Science,* 1996, **273**, 1185.
7. C. Li, J. Lin, *J. Mater. Chem*., 2010, **20**, 6831.
8. F. Wang, X. Liu, *Chem. Soc. Rev.,* 2009, **38**, 976.
9. J. C. Boyer, Frank C. J. M. van Veggel, *Nanoscale*, 2010, **2**, 1417.
10. W. Xu; S. Xu, Y. S. Zhu, T. Liu, X. Bai, B. Dong, L. Xu, H. W. Song, *Nanoscale*, 2012, **4**, 6971-6973.
11. J. W. Wang, Peter A. Tanner, *J. Am. Chem. Soc.,* 2010, **132**, 947–949.
12. W. Strek, L. Marciniak, A. Bednarkiewicz, A. Lukowiak, R. Wiglusz, D. Hreniak, *Opti Express*., 2011, **19**, 14083-14092.
13. J. W. Wang, J. H. Hao, Peter A. Tanner, *Opt Lett.* 2010, **35**, 3922-3924.
14. S. Xu, Y. S. Zhu, W. Xu, B. Dong, X. Bai, L. Xu, C. Miao, H. W. Song, *Applied Physics Express,* 2012, **5,** 102701.
15. G. S. Yi, G. M. Chow, *Advanced Functional Materials,* 2006, **16**, 2324–2329.
16. H. S. Qian, Y. Zhang, *Langmuir,* 2008, **24**, 12123-12125.
17. X. F. Yu, M. Li, M. Y. Xie, L. D. Chen, Y. Li. Q. Q. Wang, *Nano Res.,* 2010, **3**, 51–60.
18. F. Vetrone, R. Naccache; V. Mahalingam, C. G. Morgan, J. A. Capobianco, *Advanced Functional Materials*, 2009, **19**, 2924.
19. S. Schietinger, T. Aichele, H. Q. Wang, T. Nann, O. Benson, *Nano Lett.,* 2010, **10**, 134–138.
20. S. Heer, K. Kömpe, H.-U. Güdel, M. Haase, *Advanced Materials*, 2004, **16**, 2102–2105.
21. W. Xu, Y. S. Zhu, X. Chen, J. Wang, L. Tao, S. Xu, T. Liu, H. W. Song, *Nano Research,* 2013, **6**, 795-807.
22. N. Liu; W. P. Qin, G. S. Qin. T. Jiang, D. Zhao. *Chem. Commun.* 2011, **47**, 7671-7673.
23. M. Saboktakin, X. C. Ye, S. J. Oh, S. H. Hong, A. T. Fafarman, U. K. Chettiar, N. Engheta, C. B. Murray, C. R. Kagan, *ACS nano*., 2012, **6**, 8758–8766.
24. S. Fischer, F. Hallermann, T. Eichelkraut, G. von Plessen, K. W. Krämer, D. Biner, H. Steinkemper, M. Hermle, J. C. Goldschmidt, *Optics Express*., 2012, **20**, 271-282.

25. X. H. Huang, I. H. El-Sayed, W. Qian, M. A. El-Sayed, *J. Am. Chem. Soc*., 2006, **128**, 2115.
26. Y. S. Wu, J. Li; Y. B. Pan, Q. Liu, J. K. Guo, *Ceramics International*, 2009, **35**, 25–27.
27. S. S. Chang, Ch. W. Shih, Ch. D. Chen, W. C. Lai, C. R. Chris Wang, *Langmuir,* 1999, **15***,* 701-709.
28. Z. Y. Zhong, S. Patskovskyy, P. Bouvrette, J. H. T. Luong, A. Gedanken, *J. Phys. Chem. B.,* 2004, **108**, 4046–4052.
29. Y. S. Zhu, W. Xu, C. Y. Li, H. Z. Zhang, B. Dong, L. Xu, S. Xu, H. W. Song, *Applied Physics Express*, 2012, **5**, 092701-3.
30. S. Polosan, M. Bettinelli, T. Tsuboi, *Phys. Status Solidi*, 2007, **4**, 1352-1355.
31. A. M. Saad, M. B. Mohamed, Maram T. H. Abou Kana, I. M. Azzouz, *Optics & Laser Technology*, 2013, **46**, 1–5.
32. Y. Li, J. Zhang, X. Zhang, Y. Luo, X. Ren, H. Zhao, X. Wang, L. Sun, C. Yan, *J. Phys. Chem. C,* 2009, **113**, 4413.
33. A. K. Singh, K. Kumar, A. C. Pandey, O. Parkash, S. B. Rai, D. Kumar, *Appl*. *Phys*. *B*, 2011, **104**, 1035.
34. Y. Q. Lei, H. W. Song, L. M. Yang, L. X. Yu, Z. X. Liu, G. H. Pan, X. Bai, L. B. Fan, *J. Chem*. *Phys*., 2005, **123**, 174710.
35. G. V. Subba Rao, S. Ramdas, P. N. Mehrotra, C. N. R. Rao, *J. Solid State Chem.,* 1970, **2**, 377.
36. S. W. Koch, M. Kira, G. Khitrova, H. M. Gibbs, *Nat*. *Mater*., 2006, **5**, 523.
37. K. Xiao, Z. Yang, *J. Fluoresc*., 2006, **16**, 755.